Westinghouse Electric Corporation Energy Systems

Box 355
Pittsburgh Pennsylvania 15230-0355

NSD-NRC-96-4808
DCP/NRC0592
Docket No.: STN-52-003

August 30, 1996

Document Control Desk
U.S. Nuclear Regulatory Commission
Washington, D.C. 20555

ATTENTION: T. R. QUAY

SUBJECT: WESTINGHOUSE RESPONSE TO NRC REQUEST FOR ADDITIONAL INFORMATION ON THE AP600

Dear Mr. Quay:

Enclosed are Westinghouse responses to NRC requests for additional information (RAIs) on the AP600 Design Certification program. Enclosure 1 contains responses to 24 questions pertaining to the thermal-hydraulic uncertainty topic. These RAIs were provided in NRC letters dated November 27, 1995, May 21, 1996, and June 16, 1996.

These responses close, from a Westinghouse perspective, the addressed questions. The NRC technical staff should review these responses.

A listing of the NRC requests for additional information responded to in this letter is contained in Attachment A.

Please contact Cynthia L. Haag on (412) 374-4277 if you have any questions concerning this transmittal.

Brian A. McIntyre, Manager
Advanced Plant Safety and Licensing

/nja

Enclosures

cc: W. Huffman, NRC (1 copy of enclosure)
N. Liparulo, Westinghouse (w/o enclosures)

E004

2905A

Attachment A to NSD-NRC-96-4808
Enclosed Responses to NRC Requests for Additional Information

Re: Thermal-Hydraulic Uncertainty

720.279
492.9 - 492.13
492.15 - 492.32

Enclosure 1 to Westinghouse
Letter NSD-NRC-96-4808

August 30, 1996

Question 720.279

In Q720.11, the staff asked for documentation describing how the results of MAAP4 calculations compare against the results of best estimate thermohydraulic codes, like RELAP. The staff also asked Westinghouse to document the margins from core damage given by the success criteria as calculated by MAAP4 for each of the initiating event groups. The staff understands that this comparison will be performed using the NOTRUMP computer code. However, the staff further understands that NOTRUMP was not used for design basis calculations for ATWS and large LOCA events, and that MAAP cannot model ATWS and large LOCA scenarios appropriately.

The following is a clarification to Q720.11. Westinghouse should provide the results of comparison calculations for the following very small and small LOCA success path scenarios using NOTRUMP and MAAP. Westinghouse should also run comparison calculations for the following ATWS and large LOCA success path scenarios using MAAP and the corresponding design basis accident computer code. The selection of these scenarios (with the exception of ATWS) was based on Westinghouse's October 20, 1993 response to Q720.109. These success paths are assumed to lead to peak clad temperatures less than 2200°F and core uncovery.

a. Two inch small LOCA in the direct vessel injection line assuming only the following equipment is available: reactor coolant pump trip, full depressurization using one Stage 1 line and one out of two lines of the fourth stage of the ADS, 1 out of 2 accumulators, 1 out of 2 gravity injection lines, containment integrity, and reactor pressure vessel water recirculation.

b. One inch small LOCA in the pressurizer SRVs assuming only the following equipment is available: reactor coolant pump trip, 1 out of 2 CMTs, full depressurization using one Stage 1 line and 2 gravity injection lines, containment integrity, and reactor pressure vessel water recirculation.

c. Pressurizer level instrumentation line break (less than 3/4 in.) assuming only the following equipment is available: reactor coolant pump trip, 1 out of 2 CMTs, full depressurization using three out of four lines of the second and third stages of the ADS, one line of gravity injection, containment integrity, and reactor pressure vessel water recirculation.

d. Very small LOCA in the pressurizer level instrument Lines (less than 3/4 in.) assuming only the following equipment is available: full depressurization using 2 out of 2 accumulators, full depressurization using four out of four second and third stage lines of the ADS, one out of one gravity injection line, containment integrity, and reactor pressure vessel water recirculation.

e. Large LOCA in the direct vessel injection line assuming only the following equipment is available: 1 out of 2 core accumulators, 1 out of 2 gravity injection lines, reactor pressure vessel water recirculation, and containment integrity.

f. ATWS assuming only the following equipment is available: turbine trip via DAS, manual boration, two out of two pressurizer safety valves, and passive RHR.

For each scenario above, provide the following code output from the PRA and DBA code calculations:

a. Time-dependent plots of the collapsed liquid level and the mixture level in the core,

b. The total time period in which the core is uncovered,

c. Time-dependent plots of the peak clad temperature for the hottest and average fuel rods,

d. A time-dependent plot of the reactor system power,

e. Time-dependent plots of the secondary system pressure for both steam generators,

f. For each of the three phases of ADS blowdown (subcooled blowdown, two-phase blowdown, and superheated blowdown), a table listing the time of onset and completion of each phase along with the mass remaining in vessel during the depressurization transient,

g. The mass of coolant remaining in-vessel prior to reflood or core recovery, and

h. A table listing the actuation times for each passive safety feature.

The response should include a comparative analysis of the differences between the values predicted by MAAP versus the values predicted by NOTRUMP, including an explanation of the source of the differences and a discussion of their significance.

Response:

This RAI was written in June of 1994. Since that time, there have been numerous interactions between Westinghouse and the NRC relative to the MAAP4 analyses that support the PRA success criteria. Westinghouse is currently performing MAAP4 benchmarking against the NOTRUMP code, using approximately a dozen cases. The benchmarking cases have been chosen based on the considerations explained in the response to RAI 492.17. The cases identified in the above RAI are outdated due to changes in the AP600 design, the PRA success criteria, and the MAAP4 analyses. The specific analyses requested in this RAI will not be performed. The large LOCA and ATWS benchmarking cases will not be performed because MAAP4 is not used to analyze these events.

SSAR/PRA Revision: NONE

Question 492.9

The MAAP4 code was used to analyze certain accident sequences to define the automatic depressurization system success criteria for AP600 at shutdown conditions. Since MAAP4 contains many simplified models with model parameters, e.g., VFSEP, that may be derived or tuned for the thermal-hydraulic conditions from the sequences initiated at the power operating conditions, has an evaluation been made to determine the applicability of MAAP4 for the shutdown sequences analyzed? Will the MAAP4 benchmarking cover the PRA sequences for both at-power and shutdown conditions?

Response

The MAAP4 benchmarking plans are focused on scenarios that are initiated from full power. However, the benchmarking sequences are selected to cover a range of T/H conditions, including cases that experience core uncovery over three hours after shutdown. The MAAP 4 analyses that support the Shutdown PRA are only for modes of operation where the RCS is intact. Thermal-hydraulically, the response at shutdown is similar to the response from at-power, except the decay heat is much lower. The results of PRA indicate that the dominant contributors to risk during shutdown are when the RCS is in a drained-down condition.

SSAR/PRA Revision: NONE

Question 492.10

P. 54-42 states that the assumed shutdown conditions for AP600 are defined in Table 54-52, which defines Modes 3 and 4 as RCS temperature ">350°F" and "200 - 350°," respectively. This mode definition is inconsistent with the AP600 Tech Specification, which defines Modes 3 and 4, respectively, as RCS temperature ">420°F" and "200 - 420°." Please explain this difference and its acceptability.

Response

The AP600 Technical Specification was changed from 350°F to 420°F after the MAAP4 shutdown analyses were done. In the MAAP4 analyses, the initial conditions were chosen to be bounding over the possible modes being covered by the analyses, and 350°F was used. A difference of 70°F in the initial RCS temperature will not impact the conclusions of the MAAP4 analyses since the decay heat assumption is the dominating influence on analysis results. The decay heat was modelled in a conservative manner, as explained in Chapter 54 of the PRA.

SSAR/PRA Revision: NONE

Question 492.11

It is stated (p. 54-46) that the shutdown PRA analyses assume the decay heat starts at 1 percent of full power, which is higher than would be anticipated during these shutdown modes of operation, and therefore is quite conservative. P. 54-42 states that the decay heat of 1 percent of full power will be reached within 1 to 2 hours after shutdown, and is therefore bounding.

How much conservatism is in this value? What would be the effect on the core damage frequency if the initiating events that occur within 1 to 2 hours of shutdown with higher decay heat are included in the shutdown PRA?

Response

Not all success paths on event trees in the Shutdown PRA are supported by MAAP4 analyses. The MAAP4 analyses only support the sequences that require ADS actuation for successful core cooling. The event trees that include ADS actuation are ones where RCS cooling is provided by the RNS and the RCS is intact. These conditions only occur in modes 4, 5, and part of 6. These modes of operation can only occur well after 1 to 2 hours of shutdown.

The PRA impact of events occurring in the first eight hours of shutdown is discussed in the response to question 2 (#2940) from an NRC letter dated November 9, 1995. The response was provided in Westinghouse letter NSD-NRC-96-4680 dated April 1, 1996.

SSAR/PRA Revision: NONE

Question 492.12

In the MAAP4 modeling for shutdown conditions, the RNS relief valve is simulated as a hot leg break, which will open and close at the relief valve opening and closing pressures, respectively, and will deliver a break flow equal to the relief flow rate.

a. P. 54-44 states that "The RNS relief valve opens when the pressure reaches ~580 psia. It will relieve approximately 550 gpm. Although the actual valve has not been selected, most relief valves close within 5 to 15 percent of the opening pressure. In the MAAP4 model, the closing pressure was selected at 536 psia, which is 7.5 percent below the opening pressure." How would the results be affected by a closing pressure 15 percent below setpoint instead of 7.5 percent?

b. With regard to relief flow rate of 550 gpm, it is stated that "it is not known whether this prediction is consistent with the actual system response, since the MAAP4 model on the hot leg is only a rough approximation of the relief valve within the RNS. However, the only impact of the valve relief rate is on the timing on the event. The MAAP4 model just described is sufficient for the purposes of defining the automatic depressurization system success criteria." What is the basis for the conclusion that the MAAP4 model is sufficient for the purposes of defining ADS success criteria?

Response

The RNS relief valve model in question is used in the loss-of-decay-heat-removal analyses. The loss of primary coolant, and thus the potential challenge to core cooling, occurs as a result of the RNS relief valve opening. In the MAAP4 model, the opening of the relief valve was approximated with a hot leg break.

a) If the relief valve closing pressure were selected at 15% below the opening pressure rather than 7.5%, the valve would open and close with less frequency. Each time the valve opens, it would remain open for a longer period of time, allowing a larger inventory loss for that valve cycle. However, there would be fewer valve cycles because it would take longer for the RCS pressure to again increase to the opening setpoint. The overall rate of inventory loss would not be significantly different for the two cases. Should the difference in valve cycling result in faster inventory loss, the low CMT level and subsequent ADS actuation would occur sooner. Timing differences could be on the order of tens of minutes. However, the decay heat assumption used in the analyses is conservative by multiple hours. Therefore, possible minor differences in the cycling of the relief valve were not considered in the analyses.

b) The modelling of the relief valve as a break on the hot leg requires the user to specify a break area rather than a flow rate, which would be the preferred input method for a relief valve. Therefore, the RNS relief valve model is only considered an approximation. The significance of the relief valve model is that it causes the loss of primary system coolant. The simplifications in this specific model could impact the timing of the event on the order of tens of minutes. However, the decay heat assumption used in the analyses is conservative by multiple hours. This is the basis for the conclusion that the MAAP4 model is sufficient for the purposes of defining ADS success criteria.

SSAR/PRA Revision: NONE

Question 492.13

With regard to the initiating event of a break in the RNS, p. 54-44 states that, because the break and the amount of water returned to the RCS are unknown, it is assumed that the RNS pumps continue to actively pump water from the RCS until the RNS pumps trip due to voiding in the hot leg. The method used to simulate the inventory lost through the RCS is to model a break on the hot leg with a break area that changes based on the hot leg water level, and a maximum break flow rate equal to the flow rate of the RNS pumps of approximately 3500 gpm. How realistic is this break model? Does the 3500 gpm pump flow represent the largest RNS break, i.e., no break in the RNS could result in a higher break flow?

Response

The flowrate from the RNS pumps is typically 2000 gpm. The flowrate of 3500 gpm is based on the maximum pumped flowrate when there is a break in the RNS. The MAAP4 model addresses the effect of a break in the RNS, accounting for 1) the unknown location of the break through parametric cases that vary the net amount of inventory loss, 2) the tripping of the RNS pumps when the hot leg voids, and 3) the continued inventory loss through steaming when the pumped loss is stopped.

SSAR/PRA Revision: NONE

Question 492.15

Besides demonstrating the applicability of MAAP4 for evaluating the PRA sequences, it is not clear what the ultimate result of the MAAP4 benchmarking effort will be. Will a "margins" type of approach also be used, based on the comparisons between NOTRUMP and MAAP4, to help define what peak core temperature as predicted by MAAP4 can be considered "success?" Will these margins then be reflected in the overall evaluation of CDF and LRF in the baseline PRA?

Response

The MAAP4 benchmarking effort plays a role in the resolution of T/H uncertainty concerns. The ultimate results of the combined benchmarking and T/H uncertainty efforts are 1) to demonstrate that the AP600 plant response to multiple failure PRA accident scenarios is understood, and 2) to demonstrate that the AP600 success criteria have been defined robustly, so that the PRA results are not impacted by the consideration of T/H uncertainty.

The MAAP4 code is used as a screening tool in this process, because it is a fast running code and allows a broad spectrum of accident scenarios to be considered. The focus of the MAAP4 benchmarking will be on the overall plant response, and whether MAAP4 predicts the correct trends for the RCS coolant inventory. Although the peak core temperature is the acceptance criterion (< 2200°F), it is not the focal point of the benchmarking effort. If MAAP4 correctly predicts the coolant inventory trend, the calculation of the core heat-up is a second-order concern. This is due to ample margin to the PCT limit for even the most challenging core uncovery cases that are credited as successful core cooling in the PRA.

The overall evaluation of CDF and LRF in the PRA is unlikely to be impacted by the MAAP4 benchmarking. An accident sequence in the PRA is either core damage or successful core cooling, and it does not matter whether there is a large or small margin to success. However, if a new MAAP4 limitation is found during benchmarking that impacts the determination of whether a scenario is successful core cooling, the impact on the Baseline PRA and Focused PRA will be assessed. This assessment will be supplemented by work being performed for T/H uncertainty resolution [reference: Westinghouse letter to NRC, NSD-NRC-96-4781, dated July 29, 1996] that determines the risk significance of core uncovery scenarios.

SSAR/PRA Revision: NONE

Question 492.16

In discussions pursuant to Westinghouse's December 8, 1995, submittal on this subject, the staff raised several questions with regard to the "key phenomena" in AP600 PRA sequences, as represented by "Table 1" in the attachment to the April 12 letter. While the formal PIRT presented at the May 3, 1996, meeting expanded on the "Table 1" phenomena, Westinghouse has still not completely addressed the staff's previous comments. Please submit a revised PIRT that responds to those comments.

Response

The NRC's previous comment (January 18, 1996 letter) is: "MAAP4 is also used to analyze steam generator tube rupture, steamline break, and other heatup transients in addition to small break LOCA. There is no PIRT to identify important phenomena, and benchmarking of MAAP4 for these other sequences."

The key phenomena that were identified in the December 8, 1995 submittal, and the PRA PIRTs provided in the May 3, 1996 presentation, are based on accident scenarios that include actuation of ADS to mitigate the accident. ADS lines will open in accidents that experience a loss of primary coolant inventory, which causes the CMTs to drain. The loss of inventory can be due to a break within the RCS, or it can be due to the opening of the pressurizer safety valves in a loss-of-heat-sink accident. The LOCA event initiators are differentiated by break size and are modelled in separate PRA event trees. The Large LOCA (LLOCA) event tree is for breaks greater than 9", which do not need the ADS venting capacity to achieve IRWST gravity injection. All other LOCAs (which is the range analyzed with MAAP4) are within the size called "Small Break LOCA" for the SSAR Chapter 15 analyses. They are modelled in the following PRA event trees: Medium LOCA, Intermediate LOCA, DVI Line Break, CMT Line Break, Small LOCA, Steam Generator Tube Rupture, Passive Residual Heat Removal Tube Rupture, and RCS Leak.

Loss of primary coolant inventory can also occur with transient initiating events, such as steamline break. With failure of passive residual heat removal and startup feedwater, the steam generators will remove decay heat until the secondary side empties. With no removal of decay heat, the RCS will pressurize until the pressurizer safety valves open. The inventory loss through the safety valves will eventually cause the CMTs to drain, actuating ADS to mitigate the event. The time frame of this heat-up scenario is on the order of hours, and can occur from any initiating transient. Details of how the event proceeds within the first tens of minutes are not important to the loss-of-heat-sink PRA scenario. The important consideration is that the steam generators dry out, leading to the loss of primary inventory through the pressurizer safety valves.

LOCAs at the smaller end of the break spectrum can also be characterized as heat-up events. If the break is not large enough to remove decay heat and heat sinks such as the passive residual heat removal are lost, the RCS pressure may increase to the pressurizer safety valve setpoint. This scenario is illustrated with results from a 0.5" break in the May 3, 1996 presentation.

In general, the heat-up events are less challenging than the larger LOCAs because the progression of the accident is slow, allowing the decay heat to decrease significantly. The heat-up events, however, have been considered in the development of the PRA PIRTs. This is evidenced by steam generator, pressurizer and ADS 1 - 3 phenomena discussed in the PIRTs.

SSAR/PRA Revision: NONE

Question 492.17

The MAAP benchmarking cases in the April 12, 1996, Westinghouse letter, and modified by the May 3, 1996, meeting presentation, are weighted heavily toward hot leg break cases. It is not clear that the list of cases chosen will exercise all relevant MAAP models over a "spectrum of cases" as claimed by Westinghouse. Justification for the selection of cases is needed.

Response

The selection of benchmarking cases is divided into two parts. The first part is to identify a set of cases that are broad enough to test all the issues that are identified in the PRA PIRTs. For thoroughness, the goal is to confirm each issue more than once, with different break sizes. This process has identified 7 cases, as listed in the May 3, 1996 presentation.

The second part of defining benchmarking cases is to identify special issues that require confirmation of MAAP4's capability. The special issues come primarily from questions on adverse systems interactions, to confirm that additional equipment does not have an adverse impact on system response. The special issues are:

- Effect of more CMTs
- Effect of accumulator on CMT performance
- Effect of more ADS lines opening
- Effect of ADS without Stage 4 (to support partial depressurization scenarios)
- Effect of break location
- Effect of PRHR heating of IRWST

This process has identified 8 cases, as listed in the May 3, 1996 presentation.

SSAR/PRA Revision: NONE

Question 492.18

Why are the PRA PIRTs based only on SBLOCAs?

Response

See response to RAI 492.16.

SSAR/PRA Revision: NONE

Question 492.19

Are there other scenarios aside from SBLOCAs, that contribute important phenomena for inclusion in the PRA PIRT?

Response

See response to RAI 492.16.

SSAR/PRA Revision: NONE

Question 492.20

What role, if any, did OSU testing play in the PIRT development? Do the other elements of the AP600 test program contribute to development of these PIRTs? Will any attempt be made to "validate" these PIRTs?

Response

The OSU PPIRT (Plausible Phenomena Identification Ranking Table) which was developed as part of the OSU scaling report is the genesis of the Westinghouse small break LOCA PIRT. The final small break LOCA PIRT is given in the response to RAI 440.325 for NOTRUMP and reflects the iterations that have occurred from the AP600 test program and discussions with the NRC. Also, the final PIRT reflects the knowledge gained from the analysis of the AP600 tests with the NOTRUMP code that indicated which phenomena are most important for predicting the test behavior. The PRA PIRT started with the small break LOCA PIRT and made the modifications as needed for the PRA cases to reflect the effects of the loss of additional equipment. Since the PRA scenarios of interest are very close to the small break LOCA design basis, the corresponding PRA PIRT is similar to the small break LOCA PIRT. Also, since the PRA PIRT is very similar to the small break LOCA PIRT, the validation which will be performed on the small break LOCA PIRT for the NOTRUMP code will also apply to the PRA PIRT.

SSAR/PRA Revision: NONE

Question 492.21

Why is core heat transfer not ranked "high" or "important" in the PIRT? For core uncovery cases, the way in which core temperatures are calculated, including the effect of heat transfer regimes/coefficients, would appear to be important, especially since recovery is an essential part of the "success" designation for such cases.

Response

In a core uncovery situation, the fuel rods experience a dryout once the mixture level drops below the point of interest. The elevations above the dryout point are cooled by convection from the steam which is generated below the dryout point. The steam is dry except for the very small region just above the dryout point. The convection could be either natural convection or forced convection depending on the integral of the power below the dryout point which is responsible for generating the steam flow. As the rod temperatures increase, there can also be radiation heat transfer to guide tube thimbles and the steam. The heat transfer is usually so low because the steam flows are small and the steam has very little heat capacity that the fuel rods heat-up adiabatically to high temperatures, regardless of which heat transfer correlation is used.

The fuel rod responds to the cooling heat flux from the rod to the vapor as:

$$q_w = h_c (T_w - T_f)$$

If the convection heat transfer coefficient is large, the sink temperature T_f quickly approaches the fuel rod temperature such that the heat flux is very small and the fuel rod heat-up nearly adiabatically. Also, if the convective heat transfer coefficient is small, there may be a temperature difference between the fuel rod surface and the coolant but again, the heat flux is low and the fuel rod will heat-up nearly adiabatically. Therefore, the heat transfer coefficient is not a highly ranked parameter in the PIRT. However, the code must use a coefficient to calculate the fuel rod heat flux, but the uncertainty can be high since there are compensating effects of the temperature difference on the fuel rod heat flux.

These affects are described in detail in the attached paper for the analysis of the heat transfer above the two-phase froth flow from the G-2 boil-off tests.

SSAR/PRA Revision: NONE

Small Break Loss-of-Coolant Accident Analyses in LWRs

Conference Papers

Keywords:
Reactor Safety
Small Breaks
Two-Phase Flow
Computer Codes
LOCA Analyses
LWRs

Prepared by
Electric Power Research Institute
Palo Alto, California

AMERICAN NUCLEAR SOCIETY
U.S. NUCLEAR REGULATORY COMMISSION
ELECTRIC POWER RESEARCH INSTITUTE

AMERICAN NUCLEAR SOCIETY
U.S. NUCLEAR REGULATORY COMMISSION
ELECTRIC POWER RESEARCH INSTITUTE

HEAT TRANSFER ABOVE THE TWO PHASE MIXTURE LEVEL UNDER CORE UNCOVERING CONDITIONS

H. C. YEH
M. Y. YOUNG
J. S. CHIOU
T. S. ANDREYCHEK

WESTINGHOUSE ELECTRIC CORPORATION
P.O. BOX 355
PITTSBURGH, PA 15230

Abstract

The heat transfer data above the froth level of a series of 336-rod bundle core uncovering tests were analyzed and several heat transfer correlation assesed in order to recommend an appropriate heat transfer model for use in small break loss-of-coolant accident analyses.

Existing heat transfer correlation were compared using two methods: (1) Comparison of the predicted heat transfer coefficient with data. (2) Comparison of the measured rod temperature with the temperature calculated by using various correlations.

These comparisons showed that the most appropriate model was a modified form of the correlation derived from the FLECHT-SEASET steam cooling tests for rod bundles and the Yao correlation for spaces grid effects.

1. INTRODUCTION

The purpose of this work is to analyze the heat transfer data above the froth level[1] of the 336 rod bundle core uncovering tests conducted by Westinghouse in 1975[3], to compare these data with the existing correlations, and to recommend a heat transfer correlation which can be used to compute the cladding temperature of the reactor fuel rods during core uncovering in a postulated loss-of-coolant accident under small break conditions. In this paper the heat transfer correlation derived from the core uncovering tests performed at Oak Ridge National Laboratory (ORNL)[4] is compared with Westinghouse test data.

The heat transfer during core uncovering has received increasing attention after the Three Mile Island (TMI) accident[5,6], since in the TMI accident the reactor core uncovered leading to high cladding temperature and damage of reactor fuel rods to rise. In order to analyze this type of accident, it is necessary to understand the heat transfer in the uncovered, or steam blanketed portion of the core. The existing heat transfer correlations such as the Dittus-Boelter correlation, however, may not be suitable for the analysis of the reactor core rod bundle geometry, since they are derived from single tube test data. The objective of this work is to examine the existing heat transfer correlations by comparing with the available test data on core uncovery, to modify the correlation if necessary, and to recommend a correlation for small break LOCA analysis.

2. TEST DESCRIPTION

The tests will be described briefly here to permit a clear understanding of the data analysis in subsequent sections. For a detailed description the reader is referred to reference 3.

The test facility includes a test section, a pressurizer, a separator, an accumulator, and a flash chamber.

The test section consists of (see Fig. 1) a rod bundle including 336 heater rods (of which 5 rods had failed before this series of tests was initiated) of overall length of 226 inches (5.74 m) and heated length of 164 inches (4.17 m), and 25 thimbles. The normalized axial power distribution produced by the heater rods is shown in Fig. 2. There are two types of instrumented rods (Fig. 1), each having 6 thermocouple locations. The combination of these provides 12 thermocouple locations as shown in Fig. 2.

---

1 The froth level is defined as the boundary between the region of continuous gas phase and the region of continuous liquid phase [1]. It has also been called the mixture level [2].

The test was initiated by filling the test vessel to a specified level with saturated water from the accumulators or the flash chamber. The power was then turned on and the data acquisition started. The water began to boil away and generated a two-phase mixture, and the rods were slowly uncovered from the top down to lower levels. As the rods were uncovered, the temperature of the rods would suddenly increase. The power was turned off when the rod temperature reached the maximum allowable temperature of 1500°F (815°C), or when the rods were uncovered below the 69-inch (1.75 m) level. After the power was turned off, data taking continued for 30 seconds and the test was then terminated.

There were 22 tests performed with the following ranges of pressure and bundle power:

Pressure	800 psia (55.2 MPa) - atmospheric pressure
Bundle power:	1.25 - 0.25 MW

3. DATA ANALYSIS

Since the purpose of the present work is to analyze the heat transfer data above the froth level, it is necessary to locate the froth level first. The froth level can be located either from (a) the temperature versus time plots of heater rods, in which a sudden excursion of temperature indicates the uncovering time at the location of that particular thermocouple; or from (b) the pressure drop versus time plots, in which a sudden change in slope indicates the uncovering time at the location of the DP cell.

The effect of droplets can be studied from the measurement of the steam flow rate $\dot{m}_{v,\,exit}$ at the exit pipe and the rate of liquid collected $\dot{m}_{d,\,exit}$ at the separator. Conservation of mass requires that the total mass flow rate leaving the froth level should be equal to the steam flow rate at exit pipe plus the rate of liquid collected at the separator. That is

$$\dot{m}_{v,\,froth} + \dot{m}_{d,\,froth} = \dot{m}_{v,\,exit} + \dot{m}_{d,\,exit} \qquad (1)$$

The steam flow rate $\dot{m}_{v,\,froth}$ at the froth level can be computed using the power generated below the froth level. The difference $\dot{m}_{v,\,exit} - \dot{m}_{v,\,froth}$ represents the evaporation above the froth level in the bundle. Since the measured vapor temperature at the outlet of the separator and the wall temperature of the pipe at the upstream of the separator are all above the saturation temperature during the tests, there was no condensation upstream of the separator. Figure 3 shows that the difference $\dot{m}_{v,\,exit} - \dot{m}_{v,\,froth}$ is small. Therefore the liquid evaporation above the froth level is negligible. It is noted that the liquid collected is only 2 to 5 percent of the total mass flow from the bundle. Therefore the liquid carryover is small.

Because of low steam flow rate and low entrainment, the effect of droplets on heat transfer above the froth level can be neglected. This argument is supported by the experiment and the analysis of Bennett et. al. [7] who investigated the heat transfer to steam-water mixtures flowing in uniformly heated tubes in which the critical heat flux has been exceeded. They made two sets of calculations of wall temperature: one assuming no evaporation and the other assuming complete thermodynamic equilibrium. From the comparison of these calculations with wall temperature data, they observed that the condition of no evaporation was approached at los mass velocity, while the condition of complete thermodynamic equilibrium was approached at high mass velocity. In the present core uncovering tests, tne mass velocity is below their lower limit. Therefore the effect of droplet evaporation should be negligible.

It seems unlikely that the carryover liquid has fallen back into the bundle from the upper plenum, since, as will be seen in the latter section, the rod temperature data at high elevations do not indicate rewetting after uncovering.

The heat transfer coefficient at the heater rod surface can be calculated using the following equation

$$h = (q_{DATAR} - q_{rad})/(T_w - T_v) \qquad (2)$$

where q_{DATAR} is the heater rod surface heat flux obtained from the measured heater rod temperature by using the data reduction code DATARH [8], q_{rad} is the net radiative heat flux from the heater rod surface to the surrounding rods, thimbles, and steam, T_w is the heater rod surface temperature, and T_v is the steam temperature measured by the steam probes. The radiation model for computing q_{rad} is described in reference 9. The model is a multiple surface network, in which radiation to steam is calculated using emissivities and absorptivities computed with six absorption bands. In the calculation of q_{rad} the required thimble temperature T_t is either obtained from data, if available, or by solving the following equation

$$(\rho CpA)_t \frac{dT_t}{dt} = q_{rad,t} - P_t\, h\, (T_t - T_v) \qquad (3)$$

In this latter case Eqs. (2) and (3) are solved simultaneously for h and T_t. In Equation (3) $(\rho CpA)_t$ is the heat capacity of the thimble, $q_{rad,t}$ is net radiation heat flux received by the thimble from the surrounding rods and steam, and P_t is the perimeter of the thimble.

Figs. 4 and 5 plot the Nusselt number divided by one-third power of the Prandtl number, $Nu_w/Pr_w^{1/3}$, against the Reynolds number, Re_w. The Dittus-Boelter correlation [10].

$$Nu_w = 0.023\, Re_w^{0.8}\, Pr_w^{1/3} \qquad (4)$$

is also plotted for reference. In order to be consistent with the recommended correlation which is to be discussed in the following section, all

steam properties in the Nusselt number, Prandtl number, and Reynolds number in these plots are evaluated at rod surface temperature as indicated by the subscript "w" instead of conventional film temperature. The difference between the results of using these two temperatures is minor. It is seen that the Nusselt number is quite large near the froth front. It then exponentially drops to the values which are parallel to the line computed from the Dittus-Boelter correlation for high power tests in which the steam is supposed to be in turbulent flow (Fig. 4), or to constant value for low power tests in which the steam in supposed to be in laminar flow (Fig. 5). Thus the data can be fitted with the correlation of the following form

$$Nu_w = 0.023\ Re_w^{0.8}\ Pr_w^{1/3}\ C_1\ F_{froth} \quad \text{for turbulent flow}$$

$$= C_2\ F_{froth}\ Pr^{1/3} \quad \text{for laminar flow} \tag{5}$$

where C_1 is the proportional constant to the Dittus-Boelter correlation, C_2 is the constant for laminar flow, and F_{froth} is a factor accounting for the high heat transfer near the froth level as will be discussed below.

The reason for better heat transfer near froth region is probably due to the droplet effect as well as thinner thermal boundary layer due to the developing flow. When bubbles in the water reach the froth surface and burst, droplets are ejected. However, because of low steam flow rate only a few small droplets are carried up. The other droplets move up a certain distance then fall back to the surface. Some of the droplets move up higher, some move up only a short distance depending on the droplet size and ejection velocity [11]. Thus, the population of the droplets decreases with increasing distance from the froth front. Therefore, the heat transfer coefficient, and the resultant Nusselt number, also decreases with increasing distance from the froth level. The factor F_{froth} can be correlated as follows

$$F_{froth} = 1 + 5 \exp\ (-0.5\ (Z-Z_{froth})/D_e) \tag{6}$$

where Z is the elevation, Z_{froth} is the froth height, and D_e is the hydraulic diameter. Fig. 6 compares the correlation (6) with the measured values of F_{froth} for turbulent and laminar flows.

Much of the heat transfer coefficient data cannot be reduced using equation (2) due to the facts that (a) most of the steam probe data exhibit wetting of steam probes characterized by a flat temperature profile at saturation temperature for a period of time after uncovering followed by a sudden rise of temperature indicating dry-out of the water on the steam probes; (b) there are only three steam probes available at the locations 82 in. (2.08 m), 109.3 in (2.78 m), and 136.7 in (3.48 m); and (c) the accumulation of errors as the temperature difference becomes small.

Fig. 7 plots the proportional constant C_1, against the pressure for turbent flow, and Fig. 8 plots the constant C_2 against the pressure for laminar flow. It is seen that there is no clear trend with pressure.

4. HEAT TRANSFER MODEL

It is evident from section 3 that much of the heat transfer coefficient data cannot be reduced due to wetting of the steam probes for a period of time after uncovering and the accumulation of errors as the temperature difference approaches zero. An alternative approach is therefore proposed in which a predictive model of the heater rod bundle is developed, and used to evaluate several forced convection correlations.

In this model the temperatures of heater rods, thimbles, dead rods, the baffle, and steam are computed with a heat transfer correlation and the appropriate radiation model for all elevations and for the complete transient of the test. At each time step the computation starts from the froth front and moves up to the top of the bundle. The steam mass flow rate is computed by the integral of power below the froth level. The energy balance for the heater rods includes the heat generation in the rods and the heat loss of the steam, thimbles, dead rods and the baffle. No rod-to-rod radiation is considered. Therefore, the computed rod temperature should represent the mean heater rod temperature of the bundle.

Since core uncovering is a rather slow process, the following assumptions are reasonable. The temperature of a heater rod is assumed to be radially uniform and the axial conduction is negligible. The steam flow is assumed to be quasi-steady, that is, the time-independent term is negligible in comparison with the convective term and the source term in the energy equations. It is further assumed that the effect of droplets is negligible in view of the above discussion.

With these assumptions the energy equation of a heater rod is given by

$$(\Sigma \rho C_p A)_r \frac{dT_r}{dt} = q_{pow} - h P_r (T_r - T_v) - q_{rad,r} \qquad (7)$$

where $(\Sigma \rho C_p A)_r$ is the heat capacity of the heater rod, which is the sum of the heat capacities of the cladding and the filler; q_{pow} is energy of heat generation; P_r is the perimeter of the heater rod; and $q_{rad,r}$ comprises all radiation losses to the steam, the baffle, thimbles, and dead rods. The radiation model for $q_{rad,r}$ is given in reference 9.

The energy equation for steam is given by

$$\dot{m}_v \frac{dh_v}{dZ} = h P_r (T_r - T_v) + q_{rad,v} - q_{loss} \qquad (8)$$

where $q_{rad,v}$ is the net radiative heat flux from the heater rods, the baffle, thimbles, and dead rods to the steam; and q_{loss} is the convective heat loss from the steam to the baffle, thimbles, and unpowered rods. The radiation model for $q_{rad,v}$ is also given in reference 9. The steam flow rate $\dot{m}_v$ is computed using the power below the froth level. The convective heat loss q_{loss} is given by

$$q_{loss} = h P_b (T_v - T_b) - h P_t (T_v - T_t) - h P_d (T_v - T_d) \quad (9)$$

where the first term is the heat loss of the baffle, the second term is the heat loss to the thimbles, and the third term is the heat loss to the unpowered rods; and P_b, P_t and P_d are the perimeters of the baffle, the thimble, and the unpowered rods, respectively.

In order to computer the radiative heat fluxes $q_{rad,v}$ and $q_{rad,v}$ and the heat loss q_{loss}, the temperature of the baffle, thimbles, and dead rods must be calculated. The energy equations for these components are

$$(\rho C_p A)_b \frac{dT_b}{dt} = - h P_b (T_b - T_v) + q_{rad,b} \quad (10)$$

$$(\rho C_p A)_t \frac{dT_t}{dt} = - h P_t (T_t - T_v) + q_{rad,t} \quad (11)$$

$$(\Sigma \rho C_p A)_d \frac{dT_d}{dt} = - h P_d (T_d - T_v) + q_{rad,d} \quad (12)$$

The radiation model for $q_{rad,b}$, $q_{rad,t}$, and $q_{rad,d}$ are also given in reference 9. Equations (7), (8), and (10) through (12) are solved simultaneously for the temperatures, T_r, T_v, T_b, T_t, and T_d for the heater rod, steam, the baffle, the thimble, and the unpowered rod, respectively.

Due to the complex geometry of the baffle, the baffle heat transfer was modelled using the following approach:

The baffle was constructed from four honeycomb plates as shown in Fig. 1. The data shows the temperature at the outer tip of the honeycomb remained close to the saturation temperature throughout the test, while the inner temperature rose to elevated temperatures. In the present calculation, the baffle is treated as a plate having an "effective thickness". The effective thickness is adjusted for each test until the inner temperature history agrees with test data. This insures that both the convective and the radiation heat transfer to the baffle which depend on the inner temperature of the baffle, are correctly calculated.

The correlations to be compared are as follows:

1. Dittus-Boelter correlation [10]

$$Nu = 0.023 Re^{0.8} Pr^{0.4} \quad (13)$$

2. ORNL correlation [4]

This correlation is similar to that of Dittus-Boelter except that all steam properties are evaluated at the wall temperature

$$Nu_w = 0.021 Re_w^{0.8} Pr_w^{0.4} \quad (14)$$

3. McEligot correlation [12]

$$Nu = 0.021\ Re^{0.8}\ Pr^{0.4}\ (T_v/T_w)^{0.5} \qquad (15)$$

4. Correlation derived from the FLECHT-SEASET Steam cooling tests [13]

$$\begin{aligned} Nu &= 7.86\ Pr^{1/3} && Re \leq 2000 \\ Nu &= -24.551 + 0.0162\ Re)\ Pr^{1/3} && 2000 \leq Re \leq 2500 \\ Nu &= 0.0797\ Re^{0.6774}\ Pr^{1/3} && 2500 \leq Re \leq 25200 \\ Nu &= 0.023\ Re^{0.8}\ Pr^{1/3} && 25200 \leq Re \end{aligned} \qquad (16)$$

Fig. 9 compares the measured rod temperature at 136.7-inch (3.48 m) elevation and the temperature computed using the above four correlations. It is seen that the calculated rod temperature is not very sensitive to the correlation used. One can illustrate the small effect of the heat transfer correlation on the rod temperature using a heat transfer coefficient twice as large as that computed by the Dittus-Boelter correlation. The resultant temperature is still not much different from that computed by the Dittus-Boelter correlation and other correlations (Fig. 9). These unexpected results can be explained as follows. Consider a steam cooling system at steady state. Now, let the heat transfer coefficient be increased so that the convective heat flux increases. Since the heat capacity of the steam is small, the increase of heat flux causes the steam temperature to increase quickly in a short distance but the rod temperature drops only slightly because of larger heat capacity. Thus the temperature differences ΔT ($= T_r - T_v$) between the rod and the steam decreases as steam moves upward. Since the convective heat flux q_{conv} is the product of the heat transfer coefficient h and the temperature difference ΔT, that is $q_{conv} = h\Delta T$, the decrease of ΔT tends to compensate the increase of h and the resultant heat flux q_{conv} tends to remain unchanged at higher elevations. Thus, before the rod temperature at high elevations has changed appreciably, the system already reaches a new steady state where the heat flux at higher elevations is about the same as the heat flux at the previous steady state at the same elevations. Therefore, the calculated temperature is quite insensitive to the correlation used at elevations away from the froth front, but is more sensitive near the froth front (Fig. 9).

To support the above argument another extreme case has been examined. A fictitious fluid with large heat capacity (that is, large mass flow rate and specific heat) was chosen to replace the steam. The calculation results show that the rod temperature drops drastically while the fluid temperature stays near the saturation temperature as the heat transfer coefficient h is doubled (Fig. 10). It is interesting to see that even in this extreme case the change of the temperature difference ΔT almost exactly compensates the change of h so that the heat flux q_{conv} remains to be about the same, that is, as h increases two times, ΔT drops in half.

The insensitivity of the calculated rod temperature with different heat transfer coefficient can also be explained by an analytical solution of the following idealized model.

To render the problem amenable to solution, consider the case of a quasi-steady state condition; that is, an observor moving along with the froth front can detect no temporal change in temperatures of the rod and steam. The quasi-steady state can be achieved with the following assumptions:

1. The heater rod has a uniform axial power profile;

2. The total power, and hence the rate of steam generation, below the froth level remains unchanged as the froth level decreases;

3. The rate of decrease of the froth level is constant. This assumption is a consequence of assumption 2.

For the quasi-steady state just depicted the energy equations for the rod and steam in a coordinate system moving with the froth front (Fig. 11(a)) can be written as

$$(\Sigma\rho C_p A)_r V_{fr} \frac{dT_r}{dZ'} = q - h P_r (T_r - T_v), \tag{17}$$

$$(\rho C_p A)_v (V_v + V_{fr}) \frac{dT_v}{dZ'} = h P_r (T_r - T_v) \tag{18}$$

respectively. The boundary conditions are

$$T_r = T_v = T_{sat} \quad \text{at} \quad Z' = 0 \tag{19}$$

Eqs. (17) and (18) are two linear ordinary differential equations for two dependent variables T_r and T_v. If, in addition to the above assumptions, it is further assumed that $(\Sigma\rho CpA)_r$, $(\rho CpA)_v$, V_v q, and h are constant, then Eqs. (1) and (2) are linear equations with constant coefficient, and the analytical solution subject to the boundary conditions (19) can be obtained readily as follows:

$$T_r = T_{sat} + \Delta T_1 \left[1 - \exp\left\{-\frac{h P_r (b+1)}{(\Sigma\rho C_p A)_r V_{fr}} Z'\right\}\right] + \frac{1}{b+1} \frac{q'}{(\rho C_p A)_v (V_v + V_{fr})} Z' \tag{20}$$

$$T_v = T_r - \Delta T_2 \left[1 - \exp\left\{-\frac{hP_r (b+1)}{(\Sigma\rho C_p A)_r V_{fr}} Z'\right\}\right], \tag{21}$$

where

$$b = \frac{(\Sigma\rho C_p A)_r V_{fr}}{(\rho C_p A)_v (V_v + V_{fr})}, \quad \Delta T_1 = \frac{1}{(b+1)^2} \frac{q'}{h P_r}, \quad \Delta T_2 = \frac{1}{b+1} \frac{q'}{hP_r}$$

The above solution expresses the temperature T_r and T_v as functions of the moving coordinate Z'. Our interest, however, is in the expressions for T_r and T_v as functions of time for a given elevation Z. This can be accomplished by substituting the relation

$$Z' = V_{fr}\,(t - t_{fr})$$

in Eqs. (20) and (21), giving

$$T_r \cong T_{sat} + \Delta T_1 \left[1 - \exp\left\{-\frac{h\,P_r(b+1)}{(\rho C_p A)_r}\,(t - t_{fr})\right\}\right] + \frac{b}{b+1}\,\frac{q'}{(\rho C_p A)_r}\,(t - t_{fr}), \tag{22}$$

$$T_v \cong T_r - \Delta T_2 \left[1 - \exp\left\{-\frac{h\,P_r\,(b+1)}{(\rho C_p A)_r}\,(t - t_{fr})\right\}\right]. \tag{23}$$

The change of the rod temperature with different values of heat transfer coefficient h can now be studied. In the parameter b the heat capacity $\rho C_p A$ multiplied by a velocity will be called "flow heat capacity". The parameter b is the ratio of the flow heat capacities of the heater rod and the steam. Two cases in which b is assumed large and small will be examined.

Case I. Large b (small steam flow heat capacity)

This is the case with small flow heat capacity of steam as in the case of the G-2 tests. The last term in Eq. (22) dominates as shown by the dashed line in Fig. 11(b). The second term on the right-hand side of Eq. (22), which is the only term involved in h, is small because of the factor $1/(b+1)^2$ and attains an asymptotic value of ΔT, in a short time. Therefore, different values of h do not change the rod temperature T_r significantly. As for the steam temperature T_v, since ΔT_2 in Eq. (23) is proportional to the factor $1/(b+1)$, which is larger than the factor $1/(b+1)^2$ in the expression for ΔT, Eq. (23) indicates that the steam temperature is more sensitive to h than is T_r.

It is noted that both the rod and steam temperatures are more sensitive to the value of h near the froth level than further downstream as is seen from the exponential terms in Eqs. (20) and (21).

Case II. Small b (large steam flow heat capacity)

In this case the flow heat capacity of steam is large, which corresponds to the case of Fig. 10. The situation is completely reversed from the previous case. The second term on the right of Eq. (22) dominates, and reaches an asymptotic value of ΔT_1, in a short time (Fig. 11(c)). Since ΔT_1 is inversely proportional to h, as h doubles, ΔT_1 decreases by half. This is in complete agreement with previous calculation shown in Fig. 10. The steam temperature, on the other hand, is quite insensitive to the value of h as can be seen from Eq. (23) where $\Delta T_2 \cong \Delta T_1$ and the terms involving ΔT_2 and ΔT_1 cancel each other leaving the terms which are independent of h.

The analytical result of the idealized model serves to explain why the calculated rod temperature of G-2 tests does not change significantly with different heat transfer correlations used.

Since the calculated rod temperature does not change significantly with different correlations used, it is not practical to select a best correlation by comparing the rod temperature. From the above theoretic analysis it is seen that the temperature difference, ΔT, between the rod and the steam is more sensitive to the correlations used than the rod temperature. Therefore this temperature difference can be used as a criterion for selecting a best correlation. Figs. 12 and 13 compare the predicted and the measure ΔT for a high power test and a low power test, respectively, in which the steam temperature data do not show wetting of the steam probe after uncovering. In each of these figures two curves of measured ΔT are shown: one is based on the average temperature of the rod in the central zone (the central 5x5 array), the other is based on the average temperature of the rods in the middle zone (the next three rows). The later curve will be used to compare with the predicted ΔT since the predicted temperature is the average temperature of the bundle, which can be represented by the temperature in the middle zone.

For the high power test the Reynolds number is about 4000 to 5000 and the steam is in turbulent flow. Fig. 12 shows that the data lie below that predicted by the ORNL correlation and quite close to that predicted by the FLECHT steam cooling correlation. By using the FLECHT steam cooling correlation with the steam physical properties evaluated at the rod temperature (that is, wall temperature), the agreement in both the ΔT comparison (Fig. 12) and the T_r comparison is improved except at 110.7-inch (2.81 m) elevation which is still not satisfactory (this is due to the spacer grid effect as will be discussed later). Furthermore, the Nusselt number thus calculated is about 1.5 times the Nusselt number calculated with the Dittus-Boelter correlation in agreement with the results of heat transfer data reduction (that is, C_1 is about 1.5 in Fig. 7). Therefore, for turbulent flow the FLECHT steam cooling correlation with properties evaluated at wall temperature is recommended.

For the low power test the Reynolds number is about 1000 to 1300 and the steam should be in laminar flow. Therefore, several laminar-flow-type-correlations, that is, $Nu_w/Pr_w^{1/3}$ = constant = 6, 10 and 15 are plotted for comparison Fig. 13. By choosing the constant of 13.7 the agreement in both the ΔT comparison and the T_r comparison is quite good. Furthermore, this number is also in agreement with the results of heat transfer data reduction discussed previously (Fig. 8). Hence, the following correlation is recom- mended for laminar flow

$$Nu_w = 13.7\ Pr_w^{1/3} \tag{24}$$

The spacer grid and mixing vane effect can be studied by using the correlation of Yao et al. [14] in the above model. The Yao correlation for the mixing vane grid is

$$\frac{Nu}{Nu_o} = [1 + 5.55\ a_1^2 \exp\{-0.13(Z - Z_{grid})/D_e\}]$$

$$[1 + a_2^2 \tan^2 \phi \exp\{-0.034\ (Z - Z_{grid})/D_e\}]^{0.4} \tag{25}$$

where the first bracket on the right is due to blockage effect of the spacer grid and the mixing vane, the second bracket is due to the swirling effect of the mixing vane [15], and

a_1 = the blockage ratio of spacer grid and mixing vane [15] to flow channel when viewing from upstream

ϕ = the angle of the swirling or mixing vane with respect to the axial direction

a_2 = the ratio of the projected mixing vane area to the normal grid flow area as viewed from upstream

Z_{grid} = location of the downstream edge of the spacer grid

Upstream of the spaces grid, Yao et al. suggest that Nu/Nu_o be linearly interpolated between the value computed from Eq. (25) at $Z-Z_{grid} = 0$ and unity within 2 D_e of the upstream edge of the spacer grid.

For the G-2 core uncovery tests the values of these constants are $a_1 = 0.5007$ and $a_2^2 \tan^2\phi = 0.0257$. Fig. 14 shows the rod temperature computed with the above-mentioned recommended correlation and the temperature computed with this same correlation plus correlation (25) for the mixing vane grid. Fig. 14 shows that the increase of heat transfer coefficient due to the mixing vane grid as calculated by the Yao correlation greatly improves the comparison of the rod temperature at 110.7-inch (2.81 m) elevation, which is 11 hydraulic diameters downstream of the spacer grid. The effect diminishes at elevations farther away from the grids.

Figs. 15 and 16 compare the measured rod temperature and the temperature predicted by using the recommended correlations, which include the correlations for turbulent flow, laminar flow, spacer grid, and region near the froth level. The agreement of the comparisons is reasonably good except for the 2.08 m (82-inch) elevations.

5. CONCLUSIONS AND RECOMMENDATIONS

The heat transfer coefficient data in the steam cooling region above the froth level was reduced using the measured steam temperature as a sink temperature. Since the steam temperature data exhibit initial wetting of the steam probes, the steam temperature measurements were considered unreliable in some cases. For this reason a second approach was adopted.

The second approach consisted of using existing forced convection correlations with appropriate radiation models to compute the temperature of heater rods, steam, thimbles, unpowered rods, and the baffle, and comparing the calculated rod temperature with data.

This analysis revealed that the computed rod temperature was relatively insensitive to the heat transfer correlation used at upper elevations. The reason is due to the small heat capacity (low flow rate) of the steam. The difference between the rod temperature and steam temperature was compared with data in order to select the best correlation and to modify the correlation.

The following correlations are recommended for steam cooling

$$\frac{Nu_w}{F_{froth} F_{grid}} = 13.7\ Pr_w^{1/3} \qquad Re_w \leq 2000$$

$$= 0.0797\ Re_w^{0.677}\ Pr_w^{1/3} \qquad 2000 \leq Re_w \leq 25200$$

$$= 0.023\ Re_w^{0.8}\ Pr_w^{1/3} \qquad Re_w > 25200 \quad (5\text{-}17)$$

where the factor F_{froth} affects the region near the froth level as given by Eq. (6). The spacer grid effect can be calculated with the Yao correlation as given by Eq. (25).

An important result of this analysis of steam cooling above the froth level is that, if radiation is a small component of the total heat flux, large uncertainties in the calculated heat transfer coefficient (as obtained, for example, from Eq. (2)) do not necessarily result in large uncertainties in rod heat flux, if an energy balance is used to calculate the vapor temperature.

In addition, this study indicated that further studies of heat transfer during core uncovery should focus on the area just above the froth level, since this area is most sensitive to the choice of heat transfer correlation, and also exhibits behavior indicating significant effects of droplets and perhaps developing flow.

Much of the work presented in this paper was performed under Electric Power Research Institute (EPRI) Research Project RP1760-1. The authors wish to acknowledge the valuable suggestions by Dr. K. H. Sun of EPRI. In addition the authors wish to thank Dr. S. C. Yao and R. P. Vijik for their support and suggestions.

REFERENCES

1. H. C. Yeh and L. E. Hochreiter, "Mass Effluence During FLECHT Forced Reflood Experiments," Nuclear Engineering and Design 60, p. 413 (1980).

2. K. H. Sun, R. B. Duffy, and C. M. Peng, "A Thermal-Hydraulic Analysis of Core Uncovery," Presented at the 1980 National Heat Transfer Conference, ASME, Orlando, Florida, July 29-31, 1980.

3. T. S. Andrychek, "Heat Transfer Above the Two-Phase Mixture Level Under Core Uncovery Conditions for a 336 Rod Bundle-Data Report," Vol. 1, EPRI NP-1692, January 1981.

4. T. M. Anklam, "ORNL Small Break LOCA Heat Transfer Test Series 1: Rod Bundle Heat Transfer Analysis," ORNL/NUREG/TM-445, 1981.

5. Nuclear Safety Analysis Center, "Analysis of Three Mile Island-Unit 2 Accident," EPRI, NSAC-1, July 1979.

6. Kemeny et. al., "Report of the President's Commission on the Accident at Three Mile Island," Library of Congress Catalog Card Number 79-25694, 1979.

7. A. W. Bennett, G. F. Hewitt, H. A. Kearsey, and R. K. F. Keeys, "Heat Transfer to Steam-Water Mixtures Flowing in Uniformly Heated Tubes in which the Critical Heat Flux Has Been Exceeded," AERE-R5373, October, 1967.

8. J. P. Waring, E. R. Rosal, and L. E. Hochreiter, "PWR FLECHT-SET Phase B1 Data Report," WCAP-8431, Appendix A, December 1974.

9. H. C. Yeh, et. al., "Heat Transfer Above the Two-Phase Mixturte Level Under Core Uncovering Conditions - Data Analysis Report," EPRI to be published.

10. F. W. Dittus and L. M. K. Boelter, University of California Engineering Publications, Vol. 2, 1930, p. 443.

11. N. Mitsuishi, Y. Yamamoto, and Y. Oyama, "On Liquid Entrainment and its Removal," Journal of the Society of Chemical Engineers, Vol. 23, 10 (1959) AEC-tr-4225 (1961).

12. D. M. McEligot, L. W. Ormond, and H. C. Perkins, "Internal Low Reynolds Number Turbulent and Transitional Gas Flow with Heat Transfer," ASME J. of Heat Transfer, Vol. 88, 239 (1966).

13. S. Wong and L. E. Hochreiter, "Analysis of the FLECHT SEASET Unblocked Bundle Steam Cooling and Boiloff Tests," NUREG/CR-1533, or EPRINP-1460, or WCAP-9729, January 1981.

14. S. C. Yao, L. E. Hochreiter, and W. J. Leech, "Heat Transfer Augmentation in Rod Bundles Near Grid Spacers," ASME paper 80-WA/HT-62.

15. S. C. Yao, personal communication. June, 1981. Yao suggested that a_1 should also have blockage effect and should include the projected mixing vane area as can be seen by considering an extreme case when $\phi = 90°$ in which the mixing vane is obviously a blockage.

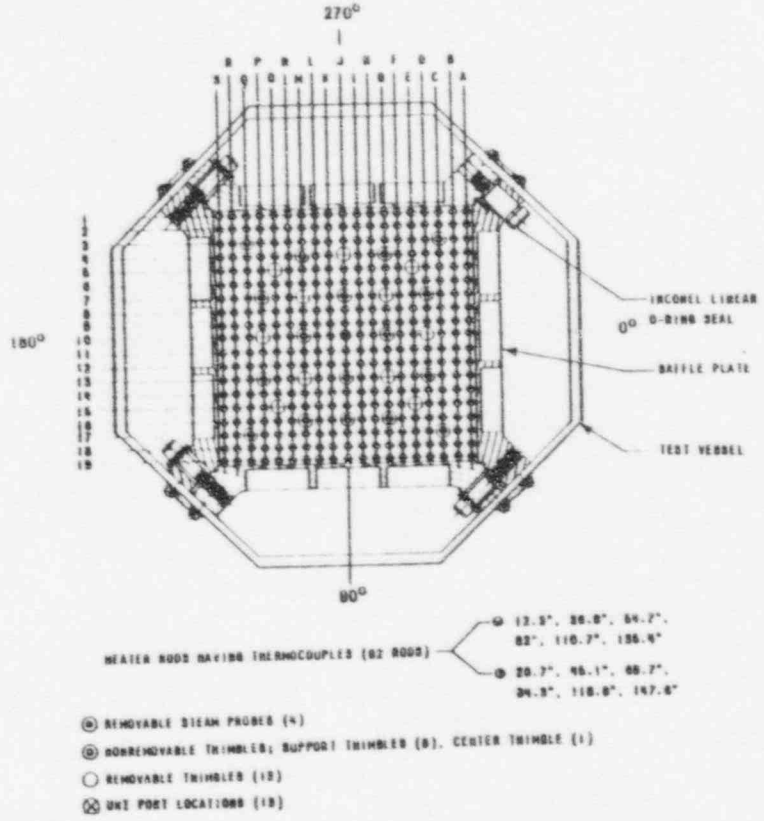

Fig. 1.G-2 Rod Bundle Baffle Cross Section And Bundle Instrumentation.

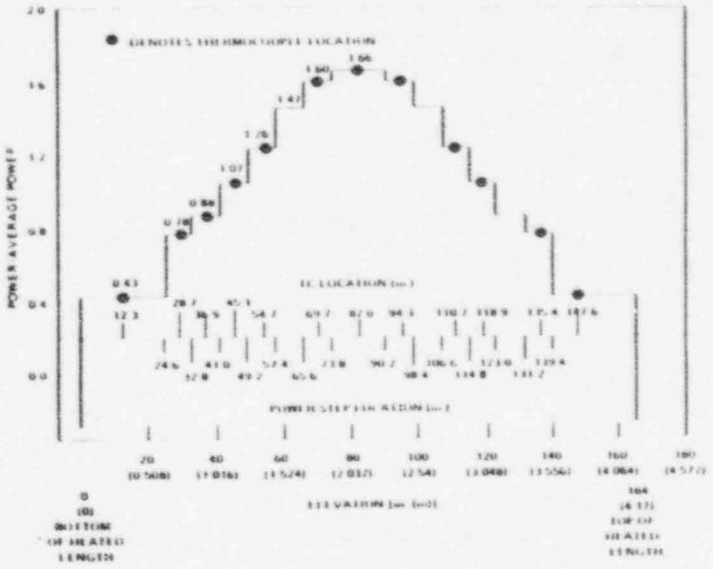

Fig. 2. G-2 Heater Rod Axial Power Profile.

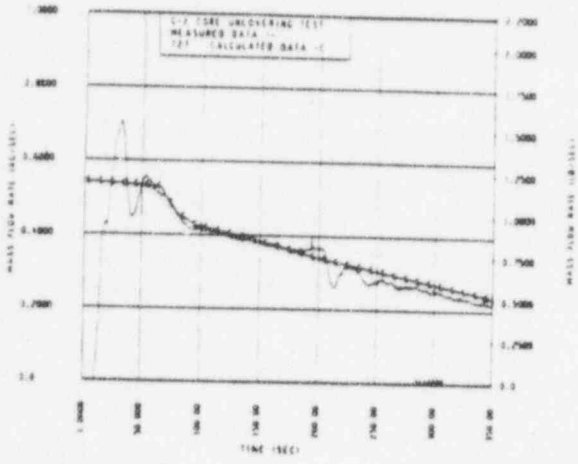

Fig. 3. Comparison of the Measured Steam Flow Rate and The Steam Flow Rate Computed From Power.

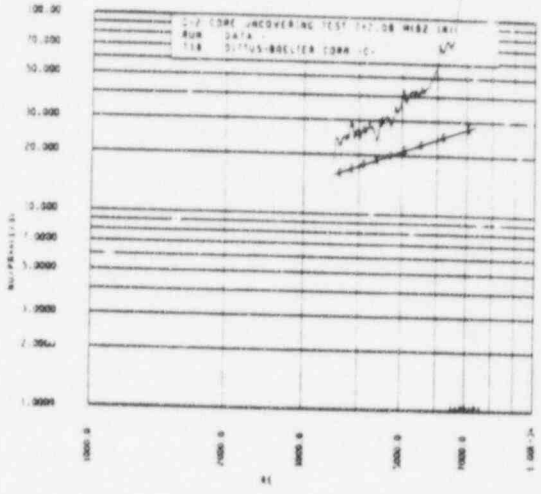

Fig. 4. Nusselt Number Divided by One-Third Power of the Prandtl Number Versus Reynolds Number for a High Power Run.

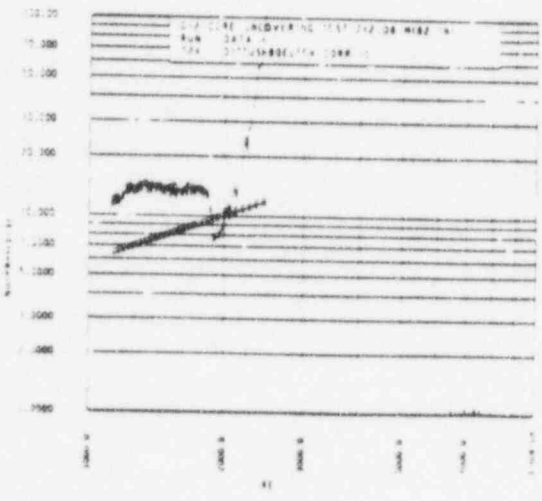

Fig. 5. Nusselt Number Divided by One-Third Power of the Prandtl Number versus Reynolds Number for a Low Power Run.

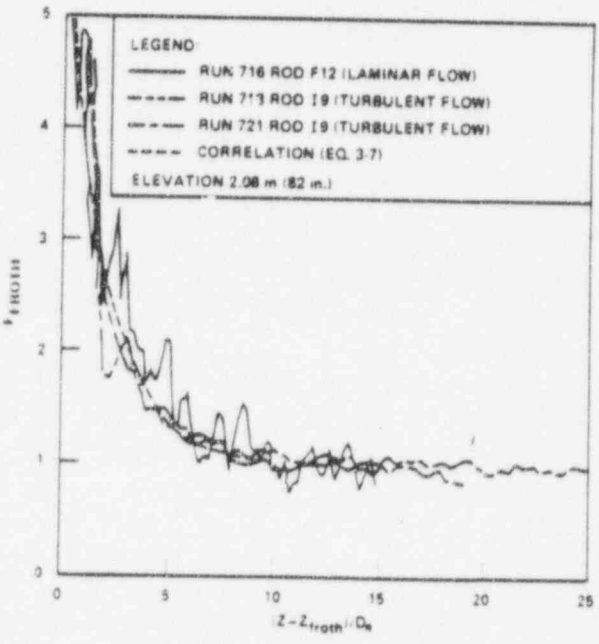

Fig. 6. Comparison of the Correlation of F_{froth} and Data.

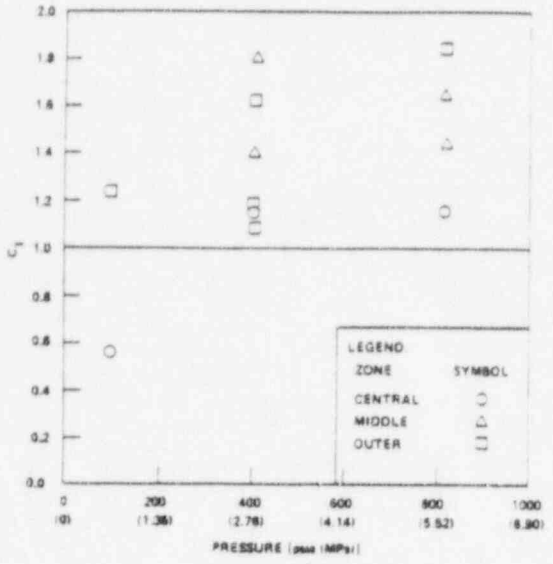

Fig. 7. C_1 Versus Pressure.

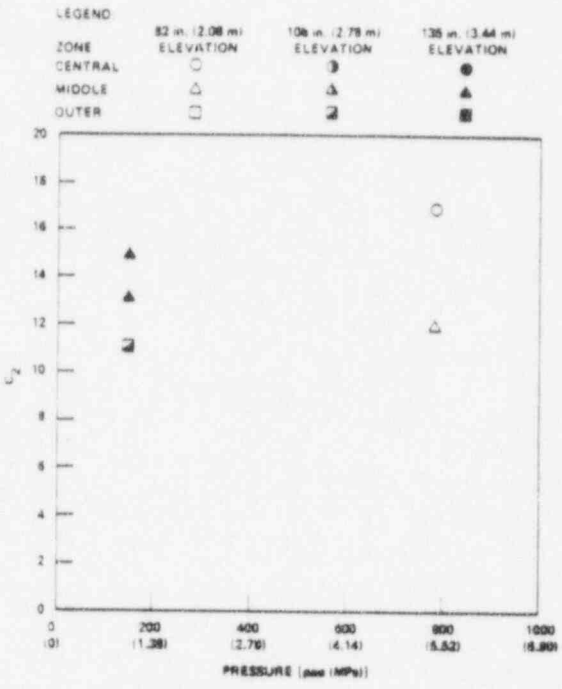

Fig. 8. C_2 Versus Pressure.

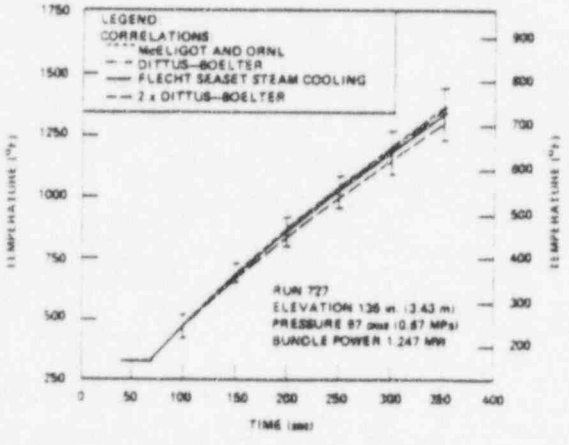

Fig. 9. Comparison of the Measured Cladding Temperature and the Temperature Predicted by Various Correlations.

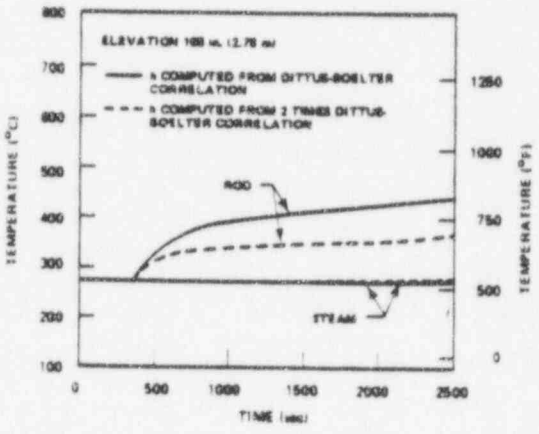

Fig. 10. Computed Temperature of the Rod and the Steam With Dittus-Boelter Correlation and Two-Time Dittus-Boelter Correlation for a Case With Hisn Capacity Fluid.

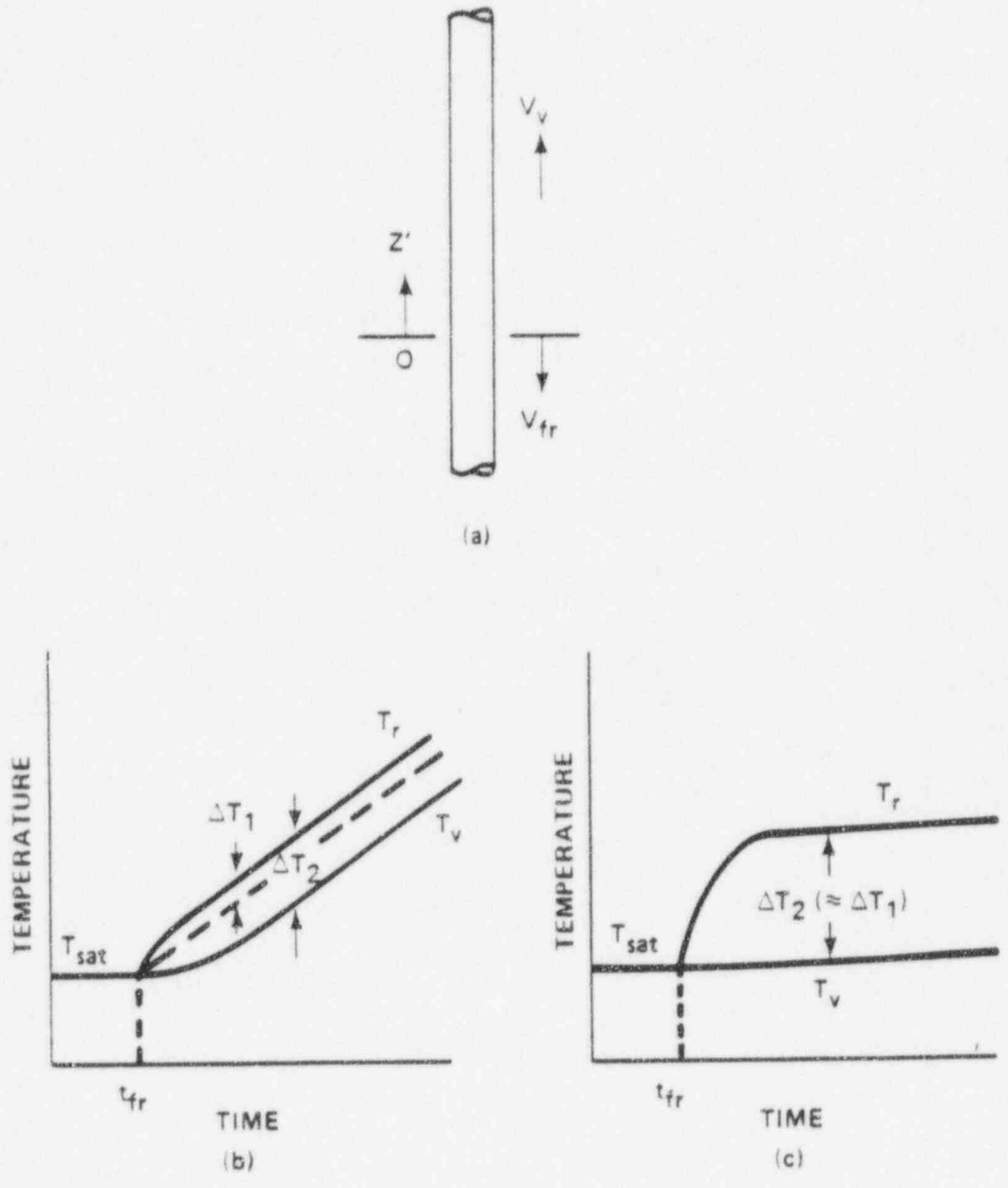

Figure 11. (a) Physical Model for the Analysis of the Core Uncovering Problem. Schematic of the Rod and Steam Temperature for (b) Small Steam Flow Heat Capacity (Large b) and (c) Large Steam Flow Heat Capacity (Small b)

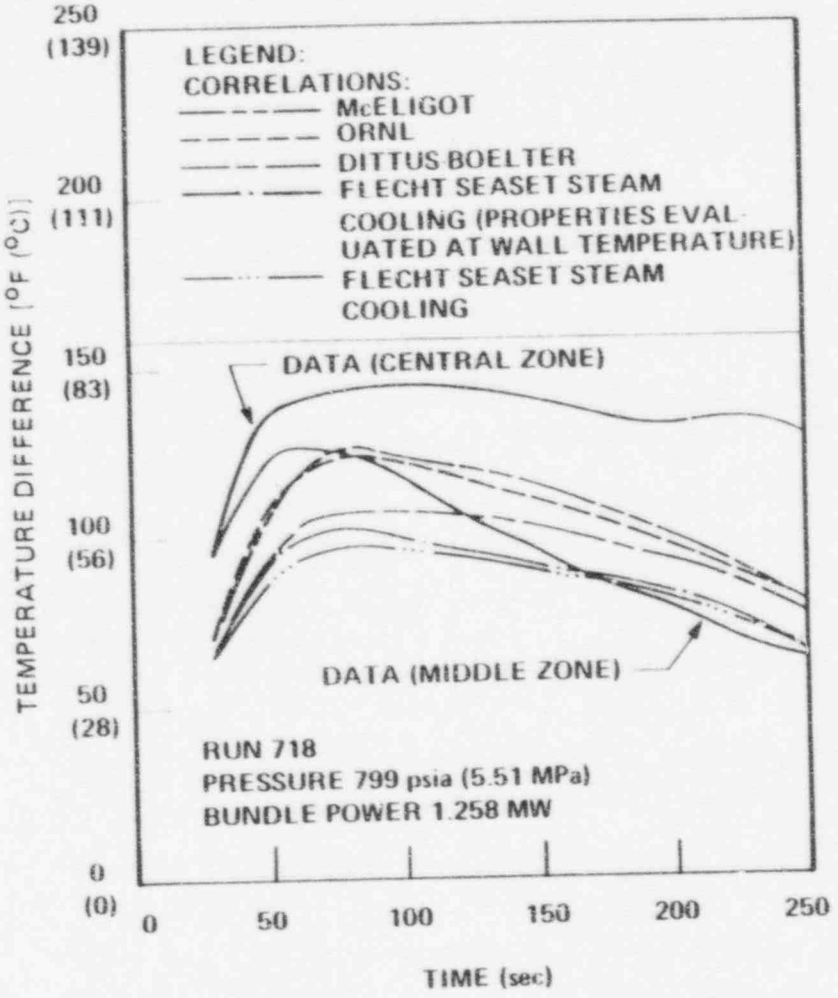

Fig. 12. Comparison of the Measured Temperature Difference ΔT ($=T_f - T_v$) and the Temperature Difference Computed With Various Correlations For Turbulent Flow.

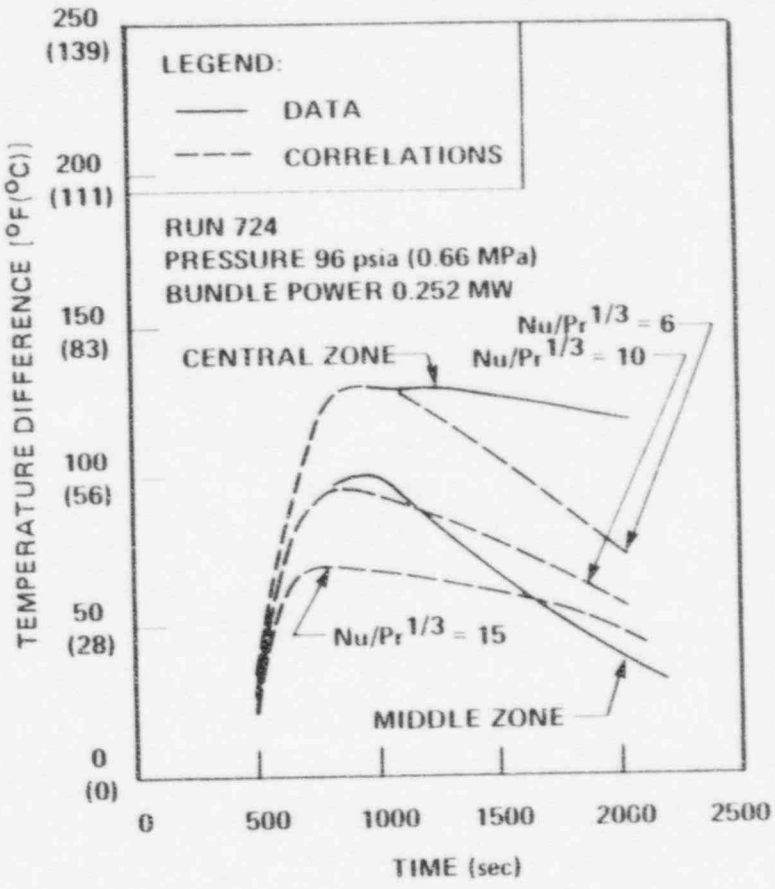

Fig. 13. Comparison of the Measured Temperature Difference ΔT ($= T_f - T_v$) And The Temperature Difference Computed With Various Correlations For Laminar Flow.

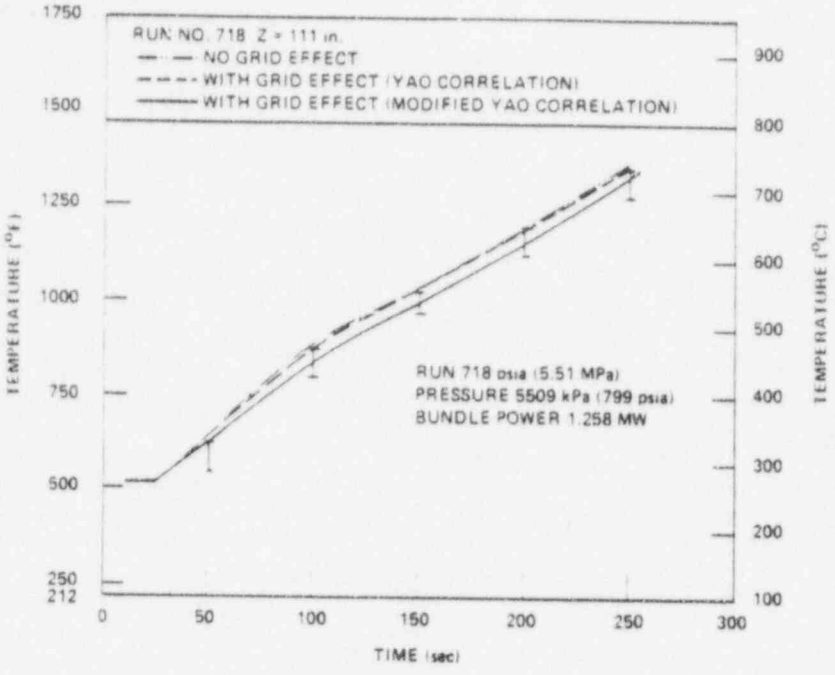

Fig. 14. Comparison of the Measured Rod Temperature Predicted Without Grid Effect and With Grid Effect (Using Yao Correlation.

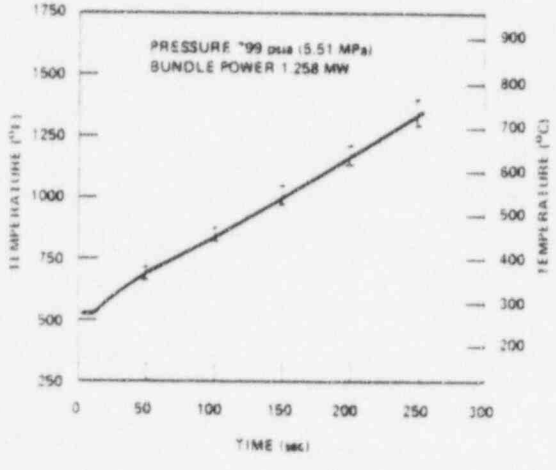

Fig. 15. Comparison of the Measured Rod Temperatured and the Temperature Predicted with the Recommended Correlation.

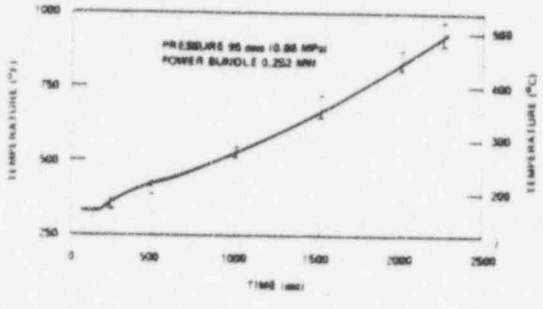

Fig. 16. Comparison of the Measured Rod Temperatured and the Temperature Predicted With the Recommended Correlation.

Question 492.22

The PIRT ranks IRWST temperature as a "high importance" parameter. However, with the prevailing assumptions of no PRHR and no (or very limited) ADS 1-3, there is no energy source to heat the IRWST water. How will this inconsistency be explained and justified?

Response

Cases for T/H analyses to support the PRA success criteria are defined with restrictive sets of equipment to cover a group of accident scenarios. Although the assumptions of no PRHR and no ADS 1-3 are prevalent in the PRA analyses, the impact of how those systems could heat the IRWST is not ignored. The IRWST water temperature has been identified as a potentially important parameter because it directly affects the heat removal capability in the core, and may have a controlling impact on the calculated minimum coolant inventory. The benchmarking exercise will substantiate the impact of the IRWST water temperature. The inconsistency of a high IRWST water temperature, when the heating sources are not credited, is a typical method used in SSAR Chapter 15 analyses to bound an accident scenario.

SSAR/PRA Revision: NONE

Question 492.23

For those sequences in which the RNS pumps are used to prevent ADS-4 actuation, it would appear that CMT temperature should be a "high importance" parameter using a rationale similar to that for IRWST temperature ranking discussed in question 492.22. Has this aspect been considered in ranking CMT phenomena?

Response

In the PRA, there is no modelling consideration of whether RNS prevents ADS-4 actuation. There are operational / cost implications with ADS-4 actuation, but there are no core damage issues dependent on RNS preventing ADS-4. Therefore, the CMT temperature is not ranked as high importance in the PRA PIRT.

SSAR/PRA Revision: NONE

Question 492.24

The break discharge coefficient is not included as an important parameter in the PIRT, apparently on the basis that changing discharge coefficient for a given break size is essentially equivalent to changing the break size itself. However, for breaks that are the size of the affected pipe or nearly that large, such as a DEG DVI-line break or an MLOCA, the discharge coefficient may be an important parameter. Staff analyses have shown that changing discharge coefficient in a DVI-line break can have a significant impact on peak cladding temperature. Please justify exclusion of discharge coefficient as an "important" parameter.

Response

As stated above, changing the discharge coefficient for a given break size is essentially equivalent to changing the break size itself. Since a range of break sizes is considered, the discharge coefficient is not judged to be an "important" parameter. The specific concern listed above for a DVI-line break will be explored further in the T/H Uncertainty Program, if this scenario is determined to be risk-significant and low-margin.

SSAR/PRA Revision: NONE

Question 492.25

Please provide the criteria that will be used to determine the MAAP/NOTRUMP comparison is "ok"?

Response

A parameter comparison between MAAP4 / NOTRUMP will be judged either as "okay" or "not okay." The assessment of "okay" will be based on whether the MAAP4 prediction shows the same trend as predicted by NOTRUMP. Any differences in the trend will be judged based on whether the deviation from NOTRUMP prediction is caused by a known, well-defined deficiency in MAAP4.

An assessment of "not okay" will be based on whether phenomena are encountered that are beyond the capability of MAAP4. This will be judged based on whether wrong conclusions would be drawn if analysis results were available from MAAP4 only.

SSAR/PRA Revision: NONE

Question 492.26

How is a phenomenological assessment of MAAP4 performed, when it is not clear that the code's models represent a phenomenological approach?

Response

The comparisons of the MAAP4 code to the NOTRUMP code for the same accident scenarios will indicate how well MAAP4 calculated the phenomena for AP600, remembering that NOTRUMP has already been compared to the AP600 separate and integral systems tests. The comparisons will guide the analysis for those areas where the MAAP4 code is simplified relative to NOTRUMP. There are modeling simplifications in the MAAP4 code which Westinghouse is fully aware of which are not based on a phenomenological approach. It is these simplifications which will be closely examined in the benchmarking activities with NOTRUMP to determine if the simplifications would lead to unrealistic conclusions based on the MAAP4 calculations.

SSAR/PRA Revision: NONE

Question 492.27

How will MAAP4 be assessed against NOTRUMP in areas where MAAP4 (lumped parameter) modeling is inconsistent with NOTRUMP's (e.g., stratification in liquid tanks), particularly if these inconsistencies relate to "high importance" phenomena?

Response

MAAP4 employs simplified noding to model some aspects of AP600's RCS. For this reason MAAP4 is being benchmarked against NOTRUMP, to confirm correct trends in its predictions. For MAAP4 models that have fewer nodes than NOTRUMP, comparisons can be made based on global conditions. For example, CMT draining effects will be examined based on the following parameters, which are identified in the PRA PIRT:

- CMT water injection flow rate
- CMT mass inventory
- CMT level
- CMT temperature
- Time draining starts

The only one of these parameters that is directly impacted by the number of nodes is CMT temperature. A single MAAP4 CMT temperature will be compared to the NOTRUMP temperatures from the top and bottom of the CMT. There will obviously be differences in the MAAP4 average versus NOTRUMP specific-location values for this one parameter. The importance of the difference will be assessed based on whether other parameters (such as CMT water injection flow rate) are impacted. The conclusion of whether MAAP4's model is sufficient will be focused on whether there is ultimately an impact on the minimum vessel inventory. The conclusion will be based on a number of different benchmarking cases, not just a single scenario.

The identification of a phenomena as "high importance" does not impact the above method. High importance phenomena are defined as ones with a controlling influence on minimum vessel inventory.

SSAR/PRA Revision: NONE

Question 492.28

How will the selection of final benchmarking cases (box #3) [be] accomplished? What criteria are used for defining the comparison process (box #4)? What criteria are used to determine if NOTRUMP is applicable to the PRA scenarios (box #5)?

Response

See the response to RAI 492.17 for the selection of benchmarking cases. See the response to RAI 492.25 for the definition of the comparison process. See the response to RAI 492.29 for the question on NOTRUMP applicability.

SSAR/PRA Revision: NONE

Question 492.29

NOTRUMP applicability (box #5) should include assessment of assumptions involved in input deck and model conditions. When assumptions are "consistent" with Chapter 15 analyses, Westinghouse must show that this is bounding for PRA sequences, with respect both to phenomenology and modeling assumptions.

Response

The application of the NOTRUMP code for the PRA assessment is still within the design basis application of the NOTRUMP code since we are using the PCT < 2200°F as the acceptance criteria for success. We will assess the input assumptions for the analysis to ensure that the code is not being used outside of its applicability.

The majority of the assumptions will be consistent with the Chapter 15 design basis calculations which will be bounding for the PRA cases. The PRA evaluation will be to examine scenarios which are similar to design basis but have reduced equipment available. It should be noted that there is a significant amount of margin in the design basis Appendix K calculations for the AP600, the core does not uncover in any of the cases analyzed. Degrading the equipment available will result in core uncovery for the small break LOCA cases, similar to that currently analyzed for operating plants. The objective of the study will be to determine if the risk significant cases yield PCTs which exceed the design basis and are therefore, not acceptable.

SSAR/PRA Revision: NONE

Question 492.30

Please elaborate on the absence of steam generator tube rupture scenarios in the presentation.

Response

The May 3, 1996 presentation was developed for a half-day meeting between Westinghouse and the NRC. The purpose of the meeting was for Westinghouse to provide details on the MAAP4 benchmarking plan, which includes the development of PRA PIRTs and the selection of benchmarking cases. An overview of PRA scenarios was given to provide a context for and further understanding of the PRA PIRTs. The overview focused on scenarios over a range of break sizes, with and without CMTs. Steam generator tube rupture scenarios were not included in the examples for two reasons. The first reason is the time constraints of the meeting. The second reason is that the PRA SGTR scenario of concern is a specialized Small LOCA, exhibiting similar system responses as a Small LOCA. The scenario of interest for MAAP4 benchmarking includes system failures, in addition to the tube rupture, that cause the accident mitigation to occur by depressurization of the primary system through automatic or manual ADS actuation. The similarities in the SGTR system response to the SLOCA scenario will be demonstrated in the benchmarking documentation.

SSAR/PRA Revision: NONE

Question 492.31

Are there scenarios in which assuming more than the minimum equipment set makes things worse? This includes:

- Adverse systems interactions
- Contributions to inventory loss, e.g., more than 2 ADS valves, especially in cases where the core is already uncovered or near uncovery?

Are there scenarios in which it is less "conservative" to assume containment isolation failure?

Response

The analyses supporting the PRA success criteria bound a group of accident scenarios with a most limiting, minimum equipment case. There are no known situations where additional equipment causes the system response to be worse. This will be confirmed through some of the benchmarking cases, as discussed in the response to RAI 492.17.

SSAR/PRA Revision: NONE

Question 492.32

The assumption of containment isolation failure causes, to some extent, a "disconnect" in the logic for following an accident past the initial phase. If containment isolation is assumed to fail, one can postulate loss of RCS inventory that exits the system as vapor and any boil-off from the IRWST. Furthermore, failure of the containment to pressurize defeats the actuation of the PCCS, so that boiled-off inventory cannot be condensed and returned to the IRWST or sump for recirculatory cooling. While the staff recognizes that long-term cooling has not yet been considered in detail as part of the T/H uncertainty effort, the staff believes this question needs to be included in the context of an overall strategy for addressing these issues. Please explain, at least conceptually, how containment isolation (or failure thereof) will be handled in these analyses.

Response

PRA Appendix A contains analyses that support the PRA success criteria. The revision submitted to the NRC in January 1995 includes analytical assumptions with the intent of bounding a group of accident possibilities. One of these bounding assumptions is that there is a failure within the largest line in the containment isolation system. The containment may still pressurize with a containment isolation failure, but the pressurization is limited in magnitude and duration. The failure of containment isolation is considered because containment isolation is not a top event on the event trees, yet it can impact the number of ADS lines that are required for successful core cooling.

Containment isolation is an issue that will be considered relative to long-term cooling and the T/H uncertainty effort. The lack of containment isolation impacts the ability to achieve successful long-term recirculation. However, the failure of containment isolation lowers the probability of an accident sequence by orders of magnitude. Preliminary quantification results of expanded PRA event trees demonstrate this (see Westinghouse letter NSD-NRC-96-4781, dated July 29, 1996). Therefore, the T/H uncertainty effort will weigh the risk significance of the failure of complete containment isolation with the impact of being able to achieve successful core cooling.

SSAR Revision: NONE